

# Effect of voltage on microstructure and corrosion resistance of microarc oxidation coatings on CP-Ti

S. Y. Chang<sup>1</sup>, H. K. Lin<sup>2</sup>, L. C. Tsao<sup>\*2</sup>, W. T. Huang<sup>3</sup> and Y. T. Huang<sup>2</sup>

The surface modification of commercially pure titanium (CP-Ti) by microarc oxidation (MAO) under different voltages was investigated using 1% $\text{H}_3\text{PO}_4$  solution as an electrolyte. The microstructure, phase composition and elemental distribution of ceramic coatings were investigated using scanning electron microscopy (SEM) and X-ray diffraction. The corrosion behaviour of the coating was also examined by potentiodynamic polarisation testing in a 3.5 wt-%NaCl solution. Micropore oxide films were formed on all the sample groups by MAO. The thickness and micropore size of the MAO coating increased with the increasing voltage. Energy dispersive X-ray spectroscopy results indicate that Ti, O and P became incorporated into the MAO coatings. At a low voltage of 250 V, the MAO coatings were composed of amorphous,  $\text{P}_2\text{O}_5$ ,  $\text{TiP}_2\text{O}_7$  and titania phases (rutile and anatase). Variation of treatment voltages increased the ceramic coatings from an amorphous structure to a phase structure, and the  $\text{P}_2\text{O}_5$  phase disappeared. The corrosion potential  $\Phi_{\text{corr}}$  of the MAO sample shifted towards nobler directions, and the corrosion density  $I_{\text{corr}}$  fell significantly compared with that of the bare CP-Ti. Corrosion testing showed that the sizes of the micropore of the MAO samples obviously decrease, and the MAO surface becomes smooth.

**Keywords:** Commercially pure titanium, Microarc oxidation, Corrosion

## Introduction

Titanium and titanium alloys are used in many applications, from aerospace to biomedical sciences. They have excellent properties, such as high specific strength, good formability, corrosion resistance and excellent biocompatibility.<sup>1-3</sup> Commercially pure titanium (CP-Ti) is an emerging titanium alloy and is widely used in the chemical, nuclear and, especially, biomedical industries.<sup>4</sup> However, poor corrosion and tribological properties greatly restrict the applications of such alloys, and therefore, they are usually used with protective coatings.<sup>5,6</sup> In recent years, many surface treatment technologies have been studied for use with titanium and its alloys, most notably anodising,<sup>7</sup> physical vapour deposition,<sup>8</sup> nitriding,<sup>9</sup> sprayed<sup>10</sup> and ion implantation surface treatment.<sup>11</sup> Recently, microarc oxidation (MAO) has been developed to provide coatings for Al, Ti and Mg components,<sup>12-14</sup> as these ceramic coatings have good wear resistance, high corrosion resistance and, especially,

good adhesion between metal and coating in comparison with the conventional anodising treatment. The treatment of biomedical titanium and titanium alloys by MAO to improve their corrosion resistance and bioactivity has been widely investigated.<sup>15-18</sup> Chen *et al.*<sup>17</sup> reported that microstructure characterisation of the oxidised  $\text{TiO}_2$  layer can be greatly affected by the discharge voltage and treatment time on  $\text{Ti}_{13}\text{Cr}_3\text{Al}_1\text{Fe}$   $\beta$ -titanium alloy during MAO treatment.

However, little has been published on the effects of discharge voltage on the characteristics and corrosion resistance of the ceramic coating, especially a coating on CP-Ti. In this study, MAO coatings were prepared in phosphoric electrolyte by applying different voltages. The morphology, microstructure, phase constituents and corrosion resistance of the MAO coatings were analysed. The corrosion behaviour was also evaluated by potentiodynamic polarisation in 3.5 wt-%NaCl solution.

## Experimental

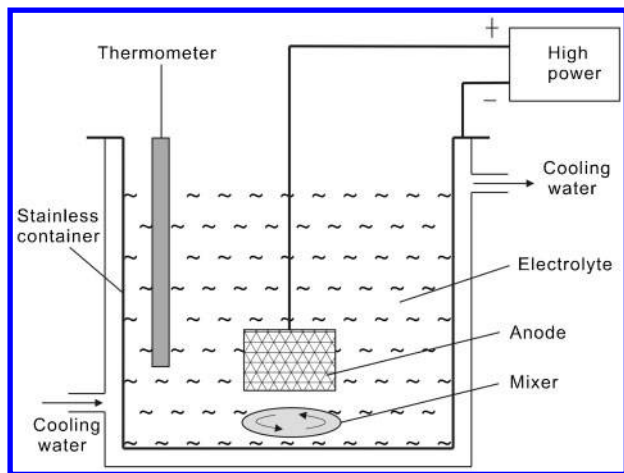
A CP-Ti having the nominal composition of 0.08 wt-%Fe, 0.02 wt-%N, 0.012 wt-%H, 0.10 wt-%O, <0.04 wt-%Si and the balance Ti was used as the substrate material for MAO coating deposition in the present study. The specimen was cut into squares 20.0 × 20.0 × 1.0 mm. After polishing and cleaning in acetone and distilled water, the specimens underwent MAO in an

<sup>1</sup>Department of Mechanical Engineering, National Yunlin University of Science & Technology, Douliu, Yunlin 64002, Taiwan

<sup>2</sup>Graduate institute of Materials Engineering, National Pingtung University of Science & Technology, Neipu, Pingtung 91201, Taiwan

<sup>3</sup>Department of Mechanical Engineering, National Pingtung University of Science & Technology, Neipu, Pingtung 91201, Taiwan

\*Corresponding author, email tclung@mail.npust.edu.tw



1 Device for MAO treatment

aqueous solution composed of electrolytes prepared with 1%  $\text{H}_3\text{PO}_4$ . During MAO treatment, the specimen was placed as the anode surrounded by a water cooled stainless steel tank as the cathode (Fig. 1). The electrolyte temperature was maintained within  $20 \pm 2^\circ\text{C}$ . The MAO coatings were produced at a constant current density of  $33 \text{ A dm}^{-2}$  for the same time period of 30 min by controlling the voltage. The applied DC voltage was varied from 250 to 350 V.

The morphology and composition of the MAO coating were examined by scanning electron microscopy (SEM; Hitachi S-4700, Japan) and energy dispersive X-ray spectroscopy (EDS; XFlash 4010 detector, Bruker, Germany). The crystal phase was analysed by X-ray diffractometry (XRD; Dmax 3-A type, Rigaku Co., Japan) using a step scan mode with a step size of  $0.02^\circ$  in the range of  $20\text{--}80^\circ$ .

Electrochemical polarisation experiments were performed using a typical three-electrode cell, no stirring and degassing of the solution at room temperature by an EG&G M273A potentiostat. The reference potential was a saturated calomel electrode (SCE) and Pt counter

electrode ( $\Phi 1.5 \text{ mm} \times 20 \text{ cm}$ ). All electrolytes were prepared by dissolving high grade chemicals in high purity deionised water ( $18 \text{ M}\Omega \text{ cm}$ ; Millipore Milli-Q SP). The specimen surfaces, with an area of  $\sim 2.829 \text{ cm}^2$ , were exposed to the 3.5 wt-% NaCl solution at  $25^\circ\text{C}$ . For dynamic polarisation testing, the potential began at  $-1.0 \text{ V(SCE)}$  and scanned in the noble direction to an anodic  $2 \text{ V(SCE)}$  at a scanning rate of  $1 \text{ mV s}^{-1}$ .

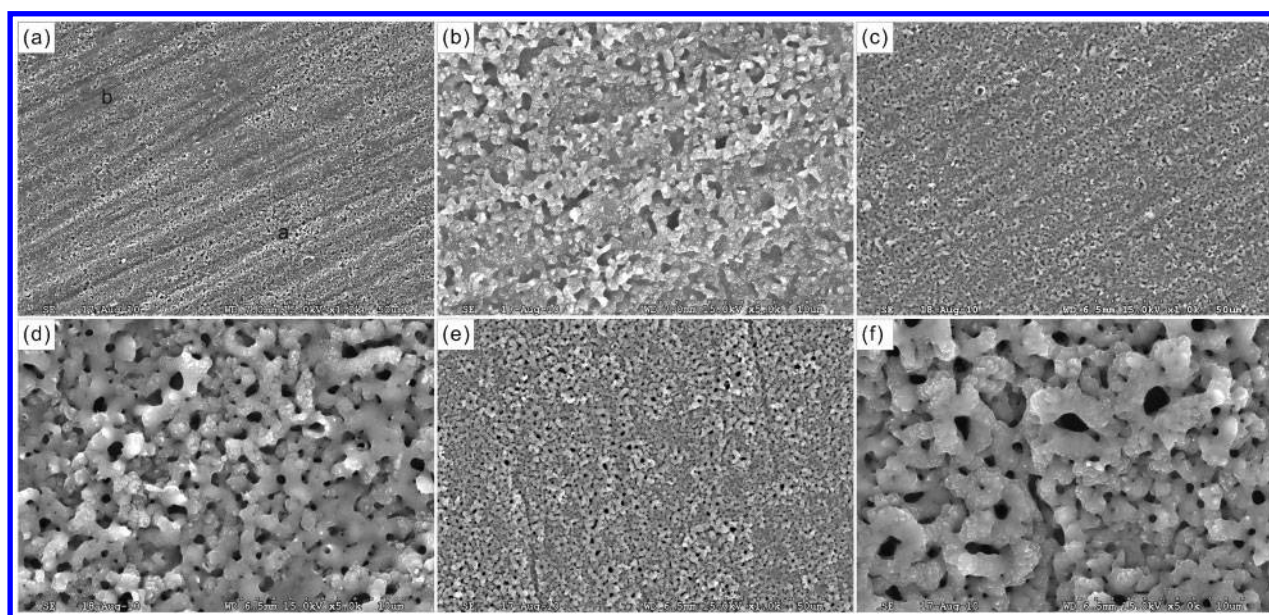
## Results and discussion

### Microstructures

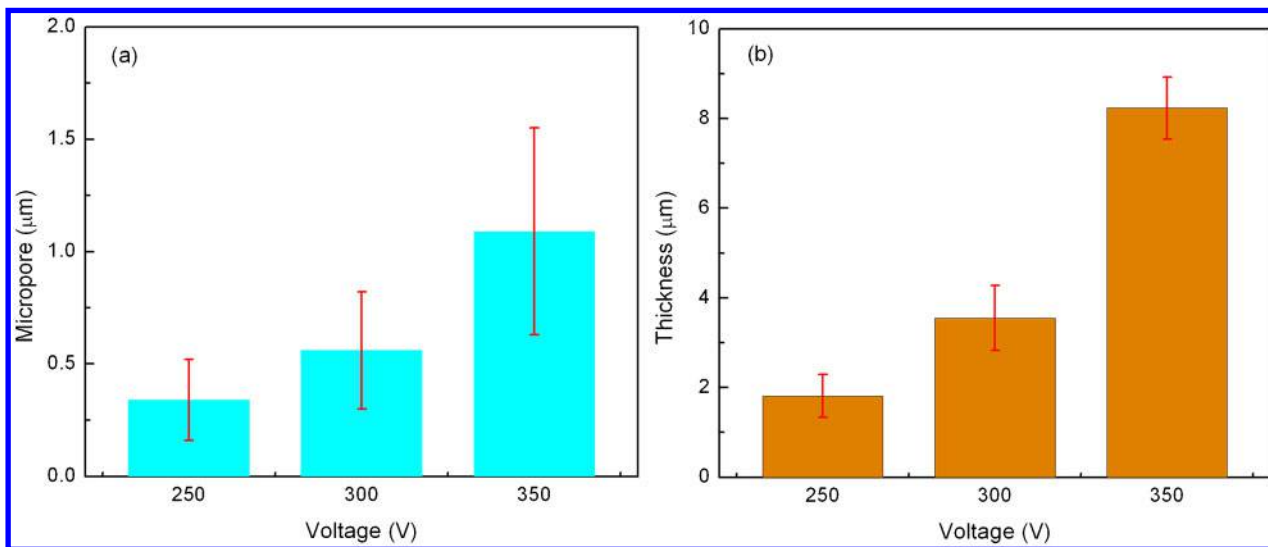
Figure 2 shows the surface morphologies of the CP-Ti after MAO using different treatment conditions. Before the oxidation treatment, only the machining grooves were observed on the surface. When a pulsed dc field of 250 V was applied, a porous oxide layer began to be formed, as shown in Fig. 2a and b. As shown in Fig. 2a, the surface morphology of the CP-Ti was inhomogeneous after oxidation at 250 V. It was composed of two distinct regions (regions a and b). In region a, oxides formed around the accumulated micropores. However, region b presented a much smoother surface. Small amounts of oxides formed in this region. Some micro-bulges in region b had regular and circular shapes with size of  $0.1\text{--}0.2 \mu\text{m}$  in diameter. Han *et al.*<sup>19</sup> reported that the MAO film matrix appears to be very dense and is composed of  $10\text{--}20 \text{ nm}$  nanocrystallised grains. Figure 3 shows the relationship between the thickness and micropore size of the MAO coatings. It can be noted that both the thicknesses and the micropores of the MAO coatings increased with increased voltage. This indicates that the higher discharge voltage led to increased sparking discharge intensity by the pulse energy, which contributes to the enlarged thickness and micropore size. A similar result was also reported by Ref. 17.

### Phase composition

Figure 4a shows a typical cross-section morphology of the MAO 300 V sample. It clearly shows that the coating was compact, with few defects (mark A), registering a



2 Surface morphologies of MAO samples formed at voltages of a 250 V (b higher magnification of a), c 300 V (d higher magnification of c) and e 350 V (f higher magnification of e)



3 a sizes of micropores and b thickness of MAO coatings formed on CP-Ti at different voltages

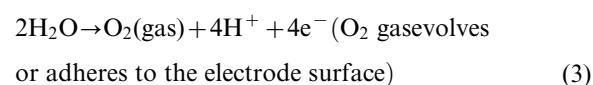
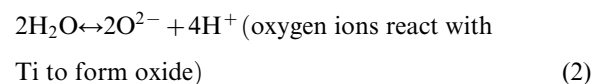
regular thickness of  $\sim 3.55 \pm 0.72 \mu\text{m}$ . Figure 4b and c displays the EDS analysis of the MAO coating surface and inner layer (Fig. 4a, mark B) on the CP-Ti respectively. Figure 5 and Table 1 show the results of EDS analysis for various MAO samples. The analysis revealed that the MAO 250 V sample mainly consisted of Ti and O, with weight concentrations of 49.92 and 47.29% respectively. Also in the surface layer was P, which came from solution anions. According to the EDS analysis, the concentrations of P and O increased with increasing MAO voltage, while that of Ti decreased steadily, as shown in Fig. 5 and Table 1. A similar result was also reported by Li *et al.*<sup>20</sup> However, P was not found in the inner MAO layer (mark B). This indicates a diffusion reaction at the Ti/TiO<sub>2</sub> interface during the MAO process.

First, the TiO<sub>2</sub> is coated during the MAO process by the following steps<sup>21,22</sup>

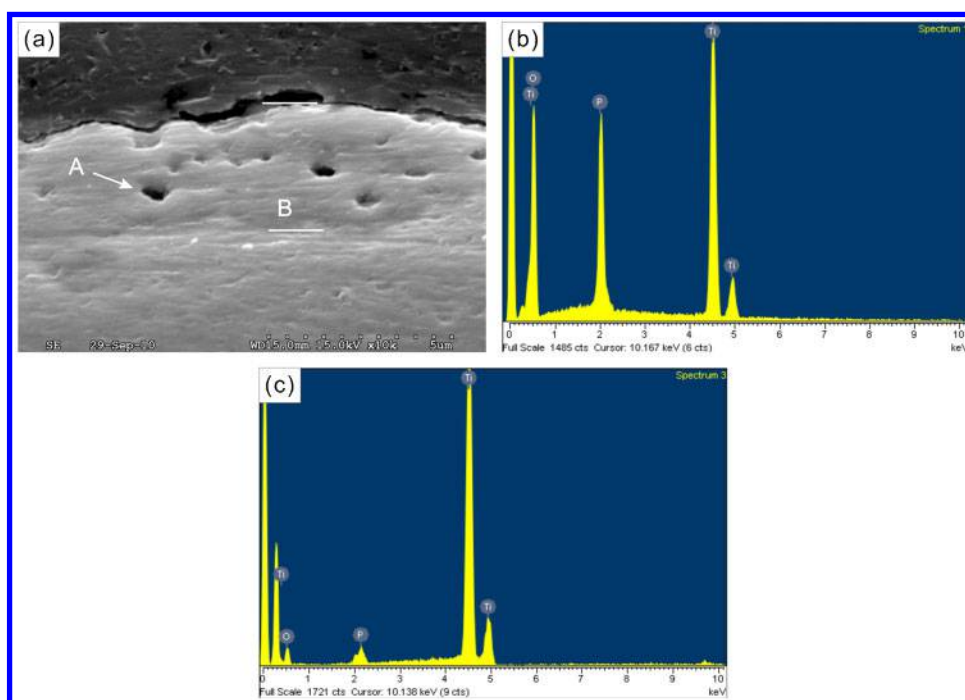
Oxide interface



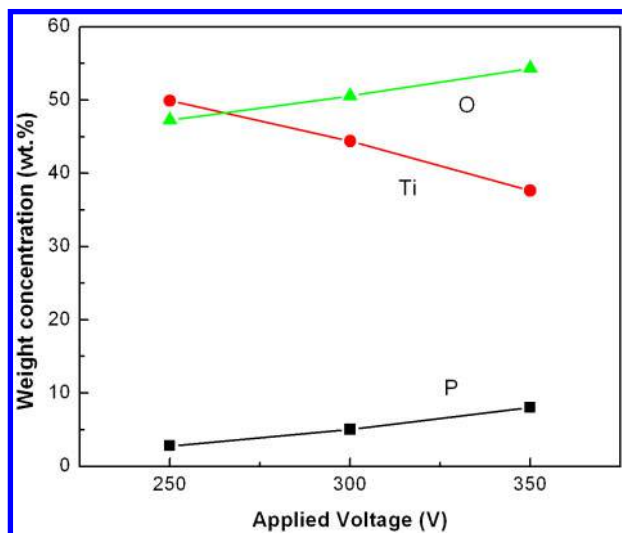
Ti oxide/electrolyte interface



Ti/Ti oxide and Ti oxide/electrolyte interface



4 a typical cross-section morphology of MAO coated CP-Ti and b EDS analysis of surface of MAO coating and inner layer (mark B) on CP-Ti



5 Chemical composition of surface layer as function of MAO voltage



Thus, the major composition of the MAO coating is  $\text{TiO}_2$ . As electrolytic anions are transmitted during anodisation, P and Ti percolate into the  $\text{TiO}_2$ . Therefore, it is considered that  $\text{TiO}_2$  and  $\text{PO}_4^{3-}$  exist as Ti and P. As shown in Fig. 4b and c, the elements Ti, O and P are distributed in the MAO coating. During the anodising process, among the mixed electrolytes

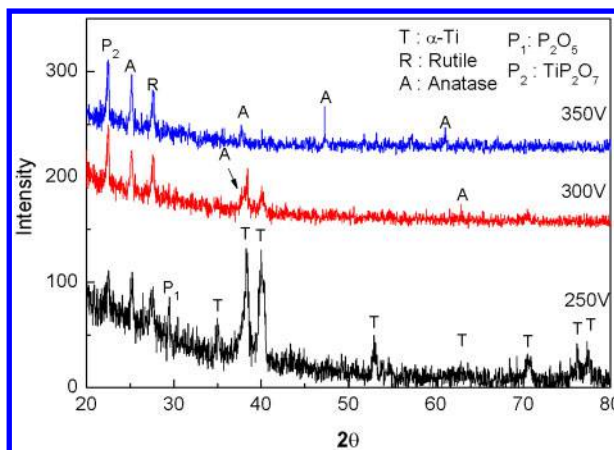


then the  $\text{H}^+$  ion migrates towards the electrolyte. Finally, it is thought that the  $\text{PO}_4^{3-}$  ion exists in the MAO  $\text{TiO}_2$  coating. It is predicted that  $\text{P}_2\text{O}_5$  and P remain in the surface and do not ionise, where the oxide film is mixed with electrolyte solution. Park<sup>23</sup> evaluated that anodic titanium oxide film for biomedical applications was synthesised by anodic oxidation in acid solution ( $\text{H}_2\text{SO}_4$  and  $\text{H}_3\text{PO}_4$ ). During anodisation,  $\text{H}_3\text{PO}_4$  was separated into  $\text{H}^+ + \text{H}_2\text{PO}_4^-$ . When the  $\text{H}_2\text{PO}_4^-$  ion was mixed in the process of film formation, the  $\text{H}^+$  ion disappeared. The incorporated phosphate species were found mostly in the forms of  $\text{HPO}_4^-$ ,  $\text{PO}_4^-$  and  $\text{PO}_3^-$ . In addition, Ti, O and P were well dispersed in the  $\text{TiO}_2$  oxide film. In addition, Li *et al.*<sup>20</sup> studied the  $\text{TiO}_2$  films for photocatalyst prepared by anodisation in acid solution (mixing  $\text{H}_2\text{SO}_4$ ,  $\text{H}_3\text{PO}_4$  and  $\text{H}_2\text{O}_2$ ). The components of the electrolyte, P and S, were found inside the photocatalyst layer as a form of  $\text{P}_2\text{O}_5$ ,  $\text{SO}_4^{2-}$ ,  $\text{TiO}_2$  (anatase and rutile) and  $\text{Ti}_2\text{O}_3$ , which were incorporated from the electrolyte into the oxide layer during anodisation. In general, at the

Table 1 Results of EDS analysis of zone indicated in Fig. 2

Specimens	Composition/wt-%			Phase identification
	Ti	O	P	
250 V (Fig. 2b)	49.92	47.29	2.78	Amorphous/anatase $\text{TiO}_2 + \text{P}_2\text{O}_5 + \text{TiP}_2\text{O}_7$
300 V (Fig. 2c)	44.41	50.57	5.02	$\text{TiO}_2 + \text{TiP}_2\text{O}_7$
350 V (Fig. 2f)	37.62	54.34	8.04	$\text{TiO}_2 + \text{TiP}_2\text{O}_7$
350 V* (Fig. 5a, mark B)	92.78	7.03	0.19	$\text{TiO}_2$

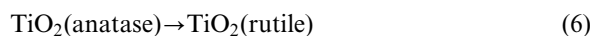
\*Results of EDS analysis of marked B zone in Fig. 5a.



6 Patterns (XRD) of a CP-Ti substrate and MAO treated at voltages of b 250, c 300 and d 350 V

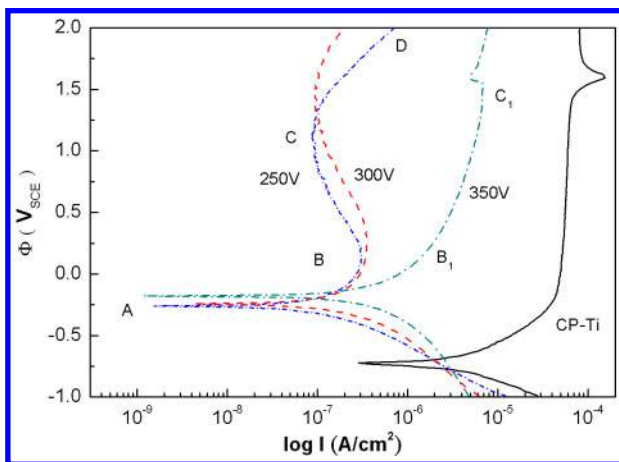
sparkling areas, a localised high temperature can be produced. The temperature at the sparking location has been evaluated at  $>1000^\circ\text{C}$ ,<sup>24</sup> and the temperature can be much higher in the centre of a sparking flame.<sup>25</sup>

Finally, possibly due to the intensive local high temperature adjacent to the coating/electrolyte interface, which results in the evaporation of water in the reaction zone,  $\text{TiP}_2\text{O}_7$  compounds were deposited on the sample surface, and the anatase  $\text{TiO}_2$  transferred to rutile  $\text{TiO}_2$ , which possibly led to the occurrence of the following reactions



Based on the above analysis, the growth of the coating is closely associated with the sparks during the MAO process; much heat is generated locally as a result, and dissolution occurs at the same time. Such heat causes the Ti ions inside the disc to move to the surface and the  $\text{OH}^-$  in the electrolyte and  $\text{O}_2^-$  ions generated from the positive pole to move into the internal disc.  $\text{TiO}_2$  is generated through the reaction of Ti ions and O ions. In this way, the oxidised film formed on the surface of the CP-Ti.

Figure 6 shows XRD patterns of MAO coatings formed on CP-Ti at different voltages. In the MAO 250 V sample, the coating was mainly composed of anatase  $\text{TiO}_2$  rutile  $\text{TiO}_2$ ,  $\text{P}_2\text{O}_5$ ,  $\text{TiP}_2\text{O}_7$  and a small amount of amorphous phase. Owing to the thinness and porosity, diffraction peaks of  $\alpha$ -Ti substrate were reflected obviously in the XRD pattern. With increasing voltage, the intensity of  $\alpha$ -Ti peaks,  $\text{P}_2\text{O}_5$  and amorphous microstructure disappeared, while that of other



**7 Polarisation curves of CP-Ti substrate and MAO coatings formed at different voltages**

peaks increased steadily. The XRD pattern for the MAO coating was composed of a large amount of anatase  $\text{TiO}_2$ , rutile  $\text{TiO}_2$  and titanium pyrophosphate ( $\text{TiP}_2\text{O}_7$ ), which was compatible with the MAO characteristics. It is reported that anodised nanotube layers can be transformed from an amorphous form into a mixture of anatase and rutile after annealing at temperatures  $>450^\circ\text{C}$ ,<sup>26</sup> which means that the MAO process can achieve suitable crystalline structures according to the application. Habazaki *et al.* reported that anodising of Ti involves an amorphous to crystalline transition in the oxide structure at relatively low voltages.<sup>27</sup> This agrees well with the results revealed by Li *et al.*,<sup>20</sup> who used pure titanium to carry out MAO treatment.

### Corrosion behaviour

The potentiodynamic polarisation curves of untreated and MAO samples in 3.5 wt-%NaCl solution are shown in Fig. 7. The corrosion potential  $\Phi_{\text{corr}}$ , corrosion current density  $I_{\text{corr}}$  and critical current density  $I_{\text{crit}}$  of the uncoated and MAO samples are compiled in Table 2. The uncoated CP-Ti substrate had a low corrosion potential [ $-541.2$  mV(SCE)] and high corrosion current density ( $2.80 \mu\text{A cm}^{-2}$ ), and its critical current density  $I_{\text{crit}}$  was rather high, up to  $37.0 \mu\text{A cm}^{-2}$ . The corrosion current densities were obtained using the TAFEL extrapolation method. It can be seen that all the MAO samples exhibited a marked shift in  $\Phi_{\text{corr}}$  towards the noble direction, and a significant one-order decrease in the corrosion current density  $I_{\text{corr}}$  and critical current density  $I_{\text{crit}}$  as compared with the uncoated CP-Ti. The improvement in corrosion property observed for MAO samples is believed to be due to the coverage of the surface of the sample by the oxide ceramic coating, which

**Table 2 Results of potentiodynamic corrosion tests in 3.5 wt-%NaCl solution\***

Specimens	$\Phi_{\text{corr}}/\text{mV(SCE)}$	$I_{\text{corr}}/\mu\text{A cm}^{-2}$	$I_{\text{crit}}/\mu\text{A cm}^{-2}$
CP-Ti	-541.2	2.80	37.0
250V-3A	-260.1	0.142	0.308
300V-3A	-210.6	0.155	0.387
350V-3A	-168.2	0.355	2.45

\* $\Phi_{\text{corr}}$  corrosion potential,  $I_{\text{corr}}$  corrosion current density,  $I_{\text{crit}}$  critical current density.

serves as a barrier layer, physically separating the substrate and the corrosive medium. In addition, for MAO samples, the corrosion resistance increased from  $-260.1$  to  $-168.2$  mV(SCE) with increased voltage. That resulted from the effect of film thickness, especially the increase in the compact MAO layer when the total film thickness increased. The compact MAO layer of film played an important role in the corrosion protection of the CP-Ti. On the other hand, it was found that the corrosion current density increased slightly, from  $1.42 \times 10^{-7}$  to  $3.55 \times 10^{-7}$   $\text{A cm}^{-2}$ . Trepanier *et al.*<sup>28</sup> reported that the quality of the coatings in terms of evenness and compactness, not the thickness, is the most important factor determining the corrosion resistance of the samples. Vangolu *et al.* reported that the most effective parameter on the corrosion current density is the voltage,<sup>29</sup> due to the surface roughness of the MAO coatings increasing with increasing voltage. Thus, the corrosion current density increased slightly. Therefore, the micropores of the MAO coatings had a detrimental effect on the corrosion performance. Larger pores increased the real exposed area to the corrosive solution and may have concentrated the corrosion medium more than little ones did.<sup>30</sup>

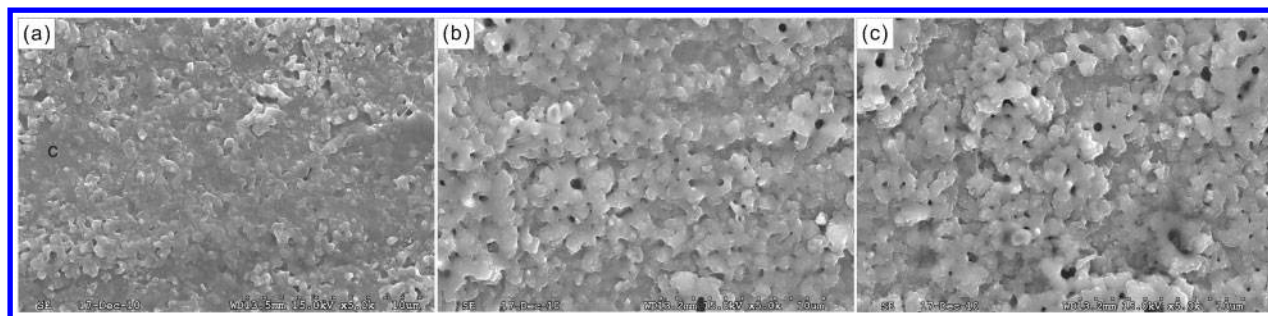
It is interesting that the anodic polarisation part consisted of several regions, namely, AB and CD. This feature could be attributed to several reactions on the electrode:  $\text{TiO}_2$  decomposition on the outer layer of MAO and the diffusion of ions through the interface between substrate and inner MAO film layer. Main reactions were thought to include



At point A, with increasing potential in the anodic direction, the outer layer of the MAO- $\text{TiO}_2$  layer dissolution occurred according to equation (1). The active dissolution of  $\text{TiO}_2$  continued with increasing potential until the  $\text{Ti}(\text{OH})_4$  concentration reached a critical value and supersaturated the surface of the MAO samples (point B). The anodic current density (point B) for the MAO sample at 250 V was found to be the maximum and to decrease with increases in potential up to C. This feature could be attributed to the reaction equation (9). However, the anodic current density of 350 V in the region ( $\text{B}_1\text{C}_1$ ) slightly increased with increases in potential. This suggests that the thickness of the MAO coating layer increasingly suppressed the diffusion of ions through the interface between the substrate and the inner MAO film layer (equation 9).

Figure 8 shows the typical morphology of the coated samples after a polarisation test. As a result, both the micropore decreased and the flat-like structure (mark c) was observed. Furthermore, the micropore density of all MAO samples decreased. Therefore, the micropore density of all MAO samples decreased. In addition, the smaller prominent particles on a ridge (Fig. 2) disappeared after the dynamic polarisation test, as shown in Fig. 8.

It is considered likely that dynamic polarisation processes occurred, leading to surface dissolution and the formation of corrosion products around the micropores, with accompanying partial obliteration of the



a 250 V; b 300 V; c 350 V

## 8 Surface morphologies of substrate and MAO coatings formed at different voltages after corrosion testing

micropores. Shi *et al.*<sup>25</sup> reported that locally dissolved areas with irregular rough surfaces were observed on MAO Ti<sub>6</sub>Al<sub>7</sub>Nb alloy after the corrosion test, and this phenomenon was attributed to the dissolution of vanadium oxide in the film, which can explain the low corrosion resistance of the MAO Ti<sub>6</sub>Al<sub>4</sub>V alloy.

## Conclusions

The effects of anodic oxidation treatment of CP-Ti on the microstructure and corrosion characteristics were investigated.

1. With increasing MAO voltage, the thickness and micropore size of the oxide layer increase, as do the concentrations of O and P in the oxide layer.

2. A low voltage of 250 V produces the MAO coatings composed of TiP<sub>2</sub>O<sub>7</sub>, titania phases (rutile and anatase), P<sub>2</sub>O<sub>5</sub>, and amorphous phase. Variation of treatment voltage increase leads to an obvious change of the ceramic coating from an amorphous structure to a phase structure, and the P<sub>2</sub>O<sub>5</sub> phase disappears.

3. Compared to the CP-Ti sample, the corrosion potential  $\Phi_{\text{corr}}$  of MAO coatings moves to a more positive potential, and the corrosion current density  $I_{\text{corr}}$  falls by one order of magnitude.

4. The corrosion resistance of MAO samples increases with increasing voltage, which is accompanied by a slight increase in the corrosion current density.

5. Corrosion testing showed that the sizes of the micropore of the MAO samples obviously decrease and the MAO surface becomes smooth.

## Acknowledgements

The authors acknowledge the financial support of this work from the National Science Council of Taiwan under project nos. NSC 101-2622-E-020-006-CC3 and NSC 101-2221-E-020-011. The authors also thank S. F. Ping for the useful discussion and sample preparation. Scanning electron microscopy was performed by the Precision Instrument Center of National Pingtung University of Science and Technology, Taiwan.

## References

1. L. C. Tsao, H. Y. Wu, J. C. Leong and C. J. Fang: *Mater. Des.*, 2012, **34**, 179–184.
2. L. C. Tsao: *Acta Phys. Pol. A*, 2012, **122A**, 561–564.

3. L. C. Tsao, R. W. Wu, M. W. Wu, C. H. Huang and R. S. Chen: *Mater. Sci. Technol.*, 2013, **12**, 1529–1536.
4. F. J. Campideli, H. E. P. Sobrinho, L. Correr, D. Goes and M. Fernando: *Dent. Mater.*, 2003, **19**, 686–691.
5. Y. M. Wang, D. C. Jia, L. X. Guo, T. Q. Lei and B. L. Jiang: *Mater. Chem. Phys.*, 2005, **90**, 128–133.
6. T. Moskalewicz, F. Smeacetto and A. Czysrska-Filemonowicz: *Surf. Coat. Technol.*, 2009, **203**, 2249–2253.
7. L. P. He, Y. W. Mai and Z. Z. Chen: *Mater. Sci. Eng. A*, 2004, **A367**, 51–56.
8. T. Schmitz, C. Hertl, E. Werner, U. Gbureck, J. Groll and C. Moseke: *Surf. Coat. Technol.*, 2013, **216**, 46–51.
9. C. Albayrak and A. Alasaran: *Corros. Eng. Sci. Technol.*, 2011, **46**, 807–811.
10. X. Zhou and P. Mohanty: *Corros. Eng. Sci. Technol.*, 2012, **47**, 145–154.
11. A. F. Yetim, A. Alasaran, A. Celik and I. Efeoglu: *Corros. Eng. Sci. Technol.*, 2011, **46**, 439–444.
12. J. Guo, L. Wang, S. C. Wang, J. Liang, Q. Xue and F. Yan: *J. Mater. Sci.*, 2009, **44**, 1998–2006.
13. L. C. Tsao: *Mater. Sci. Eng. A*, 2013, **A565**, 63–71.
14. T. H. Teh, A. Berkani, S. Mato, P. Skeldon, G. E. Thompson, H. Habazaki and K. Shimizu: *Corros. Sci.*, 2003, **45**, 2757–2768.
15. F. Liu, F. P. Wang, T. Shimizu, K. I. Igarashi and L. C. Zhao: *Surf. Coat. Technol.*, 2005, **199**, 220–224.
16. M. S. Kim, J. J. Ryu and Y. M. Sung: *Electrochem. Commun.*, 2007, **9**, 1886–1891.
17. H. T. Chen, C. H. Hsiao, H. Y. Long, C. J. Chung, C. H. Tang, K. C. Chen and J. L. He: *Surf. Coat. Technol.*, 2009, **204**, 1126–1131.
18. K. C. Kung, T. M. Lee and T. S. Lui: *J. Alloys Compd.*, 2010, **508**, 384–390.
19. Y. Han, S. H. Hong and K. W. Xu: *Mater. Lett.*, 2002, **56**, 744–747.
20. L. H. Li, Y. M. Konga, H. W. Kima, Y. W. Kima, H. E. Kima, S. J. Heob and J. Y. Koak: *Biomaterials*, 2004, **25**, 2867–2875.
21. D. M. Brunette, P. Tengvall, M. Textor and P. Thomsen: 'Titanium in medicine', 247–255; 2001, Berlin, Springer.
22. T. Y. Park, S. H. Eom, M. D. Kim, S. H. Kim, H. L. Kim, G. R. Jeon, H. J. Shin and J. W. Shin: *OSSTEM Implant System*, 2005, 506–517.
23. S. J. Park: *Met. Mater. Int.*, 2008, **14**, 449–455.
24. J. Yahalom and J. Zahavi: *Electrochim. Acta*, 1971, **16**, 603–607.
25. Z. M. Shi, G. L. Song and A. Atrens: *Corros. Sci.*, 2006, **48**, 1939–1959.
26. J. M. Macak, H. Tsuchiya, A. Ghicov and P. Schmuki: *Electrochem. Commun.*, 2005, **7**, 1133–1137.
27. H. Habazaki, K. Shimizu, S. Nagata, P. Skeldon, G. E. Thompson and G. C. Wood: *Corros. Sci.*, 2002, **44**, 1047–1055.
28. C. Trepanier, M. Tabrizian, L. H. Yahia, L. Bilodeau and D. L. Piron: *J. Biomed. Mater. Res.*, 1998, **43**, 433–440.
29. Y. Vangolu, E. Arslan, Y. Totik E. Demirci and A. Alasaran: *Surf. Coat. Technol.*, 2010, **205**, 1764–1773.
30. Y. Yang and H. Wu Hua: *Trans. Nonferrous Met. Soc. China*, 2010, **20**, s688–s692.